Journal of Power Sources 218 (2012) 119–127

Contents lists available at SciVerse ScienceDirect

Journal of Power Sources

journal homepage: www.elsevier.com/locate/jpowsour

Intermediate-temperature nickel–yttria stabilized zirconia supported tubular solid oxide fuel cells using gadolinia-doped ceria electrolyte

Seung-Young Park [a], Chan Woong Na [a], Jee Hyun Ahn [a], Ui-Jin Yun [b], Tak-Hyoung Lim [b], Rak-Hyun Song [b], Dong-Ryul Shin [b], Jong-Heun Lee [a,*]

[a] Department of Materials Science and Engineering, Korea University, Anam-dong, Sungbuk-ku, Seoul 136-713, Republic of Korea
[b] Advanced Fuel Cell Research Center, Korea Institute of Energy Research (KIER), Daejeon 305-343, Republic of Korea

HIGHLIGHTS

- Highly sinterable GDC powders were prepared by carbonate coprecipitation.
- A Ni–YSZ-supported tubular SOFC cell with Ni, Ni–GDC, GDC, and LSCF-GDC/LSCF layers was fabricated.
- The prepared cell showed a maximum power density of 594 mW cm^{-2} at 600 °C.
- This study demonstrates the potential for fabrication of a tubular SOFC at a lower sintering temperature.

ARTICLE INFO

Article history:
Received 13 April 2012
Received in revised form
12 June 2012
Accepted 13 June 2012
Available online 28 June 2012

Keywords:
Solid oxide fuel cells
Tubular solid oxide fuel cells
Gadolinia-doped ceria
Nickel–yttria stabilized zirconia
Carbonate coprecipitation

ABSTRACT

Gadolinia-doped ceria (GDC, $Gd_{0.1}Ce_{0.9}O_{1.95}$) powders with high sinterability are prepared by carbonate coprecipitation and applied in the fabrication of Ni–YSZ (yttria-stabilized zirconia)-supported tubular solid oxide fuel cells (SOFCs) with a cell configuration of Ni–YSZ/Ni/Ni–GDC/GDC/LSCF($La_{0.6}Sr_{0.4}Co_{0.2}Fe_{0.8}O_{3-\delta}$)–GDC/LSCF. A high power density (594 mW cm^{-2}) at 600 °C is achieved using the cell (diameter: 6 mm) prepared by sintering of the electrolyte at 1400 °C. This result is attributed to the dense electrolyte and good adherence between GDC and the electrode. The carbonate-derived GDC powders can be sintered to 97% of the theoretical density even at 1050 °C, which demonstrates that the fabrication temperature of tubular SOFCs can potentially be lowered by using cost-effective Ni–YSZ supports.

1. Introduction

The electrochemical conversion of hydrocarbons into electricity using solid oxide fuel cells (SOFCs) promises high energy conversion efficiency and low pollutant emission, as well as the flexible use of fuels [1]. SOFCs can be divided into two different categories according to the shape of the cell: planar and tubular SOFCs. Tubular SOFCs are very reliable and thus attractive for commercialization on account of the high mechanical strength of their supporting materials and their facile and/or tight gas sealing, scalability, and high stability against thermal cycles although the deterioration of the power density due to the elongated current path remains an obstacle [2].

The operation of tubular SOFCs in the intermediate (600–800 °C) or low (450–600 °C) temperature regimes enhances the operational stability of the cells and enables the use of cost-effective gas sealing or interconnecting materials. In SOFCs using yttria-stabilized zirconia (YSZ) as the electrolyte, the operation temperature can be reduced to 700–850 °C by thinning the electrolyte layer to 5–15 μm using an anode-supported design [3]. The operation temperature can be further decreased to <600 °C by employing highly conductive solid electrolytes such as gadolinium-doped ceria (GDC, $Gd_{0.1}Ce_{0.9}O_{1.95}$) or strontium- and magnesium-doped lanthanum gallate (LSGM, $La_{1-x}Sr_xGa_{1-y}Mg_yO_{3-\delta}$) [3].

Suzuki et al. [4] fabricated a micro-tubular SOFC (diameter: 0.8 mm) using GDC and Ni–GDC as the electrolyte and anode support, respectively, and demonstrated its high power density (1017 mW cm^{-2}) at 550 °C. Ni–YSZ composites are more cost-effective supporting materials than Ni–GDC composites.

* Corresponding author. Tel.: +82 2 3290 3282; fax: +82 2 928 3584.
E-mail addresses: jongheun@korea.ac.kr, leejongheun@gmail.com (J.-H. Lee).

0378-7753/$ – see front matter © 2012 Elsevier B.V. All rights reserved.
http://dx.doi.org/10.1016/j.jpowsour.2012.06.078

Although Sahibzada et al. [5,6] have fabricated a planar Ni–YSZ/GDC/LSCF ($La_{0.6}Sr_{0.4}Co_{0.2}Fe_{0.8}O_{3-\delta}$) cell, the power density at 650 °C was relatively low (140 mW cm^{-2}). This can be attributed to the formation of a highly resistive second phase at the interface between GDC and Ni–YSZ due to the interdiffusion of GDC and YSZ during the high-temperature sintering process. These results indicate that the fabrication of high-power-density Ni–YSZ-supported tubular SOFCs using GDC electrolytes at intermediate temperatures remains a challenging issue.

In this study, Ni–YSZ-supported tubular SOFCs using GDC solid electrolytes are fabricated by inserting a Ni functional layer and a Ni–GDC anode layer between the Ni–YSZ support and GDC electrolyte layer to prevent the reaction between YSZ and GDC. The power densities of these SOFCs are then measured. The main focus of the study is directed at the design of high-performance tubular SOFCs using cost-effective Ni–YSZ supports.

2. Experimental

2.1. Powder preparation

The GDC ($Gd_{0.1}Ce_{0.9}O_{1.95}$) powders were synthesized by carbonate coprecipitation according to the method suggested by Li et al. [7]. $Ce(NO_3)_3 \cdot 6H_2O$ (Kanto Chemical Co. Ltd., Japan) and $Gd(NO_3)_3 \cdot 6H_2O$ (Kanto Chemical Co. Ltd., Japan) were used as the source materials, and $(NH_4)_2CO_3$ (Sigma–Aldrich, USA) was used as the precipitant. The carbonate precursors were prepared by the "reverse strike" method (the addition of the mixed source solution to the precipitant solution) to achieve a more uniform cation distribution by instantaneous precipitation. Stoichiometric amounts of each component of GDC were dissolved in distilled water, after which 250 ml of a mixed aqueous solution ($[Ce^{3+}] = 0.09$ M, $[Gd^{3+}] = 0.01$ M) was dripped slowly into 250 ml of $(NH_4)_2CO_3$ aqueous solution ($[(NH_4)_2CO_3] = 0.5$ M). During the precipitation, the solution was stirred gently and the solution temperature was kept at 60 °C. The precipitates were washed with distilled water and ethanol and then dried for 24 h at room temperature. After pulverization, the precipitates were calcined at 700–900 °C for 2 h. In order to study the densification of GDC, the GDC powders were compacted into a disk-shaped specimen, isostatically pressed at 150 MPa, and subsequently sintered at 1050–1400 °C for 5 h in air atmosphere. The apparent density was measured using the Archimedes method.

2.2. Cell fabrication

A NiO–8YSZ (8 mol% yttria-stabilized zirconia) composite powders (NiO:8YSZ = 40:60 by vol%) were prepared by mixing 8YSZ powders (TZ-8Y, Tosoh Co., Japan) and NiO powders (J. T. Baker Co., USA). The NiO–8YSZ composite powders and activated carbon (pore former) were weighed and mixed in ethanol by ball milling for 14 days and then dried. Organic binder and 25 wt% of distilled water were added to the dried powders and the mixture was homogenized to form a paste. The paste was extruded in the form of a tube and dried at 120 °C for 12 h. The NiO–YSZ tubular support was prepared by heat treatment of dried tubular structure at 1100 °C.

The NiO functional layer was coated onto the porous NiO–YSZ tubular support by dip-coating the support in the slurry. The slurry for NiO coating was prepared according to the following procedure: NiO powders were added to solvent mixtures of toluene and 2-propanal. After addition of sorbitan trioleate (dispersant) and Triton X-100 (surfactant), the slurry was ball-milled for 24 h. Subsequently, di-*n*-butyl phthalate and polyvinyl butyral were added as a plasticizer and binder, respectively, and the slurry was ball-milled again for 24 h. Activated carbon (3 wt.% of the solid content) was added as a pore former.

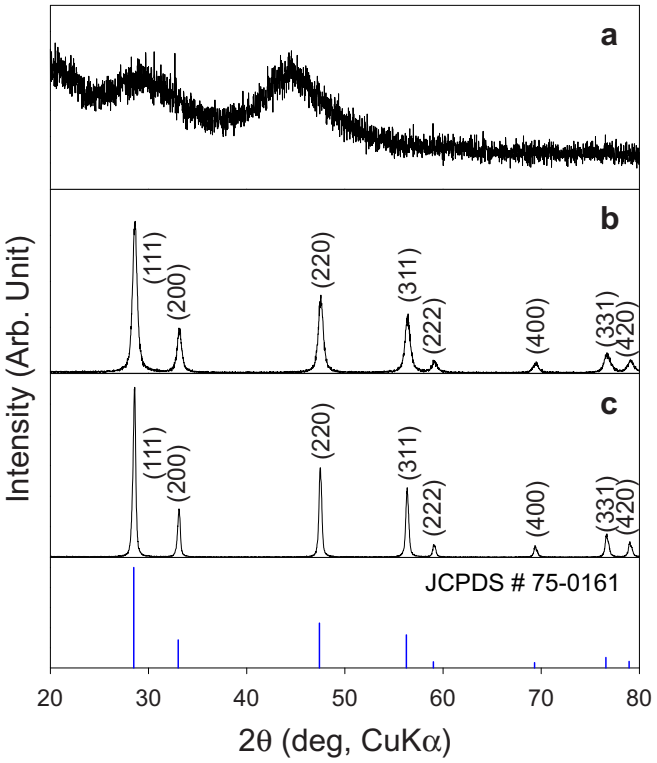

Fig. 1. XRD patterns of (a) as-prepared carbonate precursors, (b) GDC powders calcined at 700 °C for 2 h, and (c) GDC powders calcined at 900 °C for 2 h.

The NiO–YSZ tubular support was immersed in NiO slurry for 10 s, pulled out slowly, and dried at room temperature. The falling and pulling speeds were 110 mm min^{-1} and 10.6 mm min^{-1}, respectively. The green NiO film was heat-treated at 1100 °C for 3 h to obtain the mechanical strength necessary for handling. NiO–GDC functional layer was also formed by dip-coating the specimen in NiO–GDC slurry. NiO (J. T. Baker Co., USA) and $Gd_{0.1}Ce_{0.9}O_{1.95}$ (GDC, Anan Kasei Co., Japan) powders were used as solid content in the NiO–GDC slurry. The NiO and GDC powders were mixed in a weight ratio of 50:50. After being coated with the NiO–GDC green layer, the tubular structure was heat-treated at 1100 °C for 3 h.

The GDC electrolyte layer was also coated onto the support by dip coating. For this, GDC powders prepared via carbonate coprecipitation were used. Activated carbon was added to slurries of Ni and Ni–GDC to prepare a porous structure, while no carbon was added to the GDC slurry to achieve a gas-impermeable and dense GDC electrolyte layer. The GDC layer was coated twice by dip coating, drying, and heat-treating the specimen at 400 °C for 2 h. The resultant cell was sintered at 1300–1400 °C for 5 h. The cathode was formed according to the following procedure: The $La_{0.6}Sr_{0.4}Co_{0.2}Fe_{0.8}O_{3-\delta}$ (LSCF, Fuel cell materials Co., USA)-$Gd_{0.1}Ce_{0.9}O_{1.95}$ (GDC, Anan Kasei Co., Japan) composite layer was coated on the GDC electrolyte by dip coating and dried, and then the LSCF layer was coated by dip coating and dried. Finally, the cell was heat-treated at 1150 °C for 3 h to burn off all organic content to form a single NiO–YSZ/NiO/NiO–GDC/GDC/LSCF–GDC/LSCF tubular cell.

2.3. Measurement of fuel cell performance

Before measuring the cell performance, the cell was reduced by flowing 10 sccm of H_2 through the quartz tube at 600 °C for 3 h.

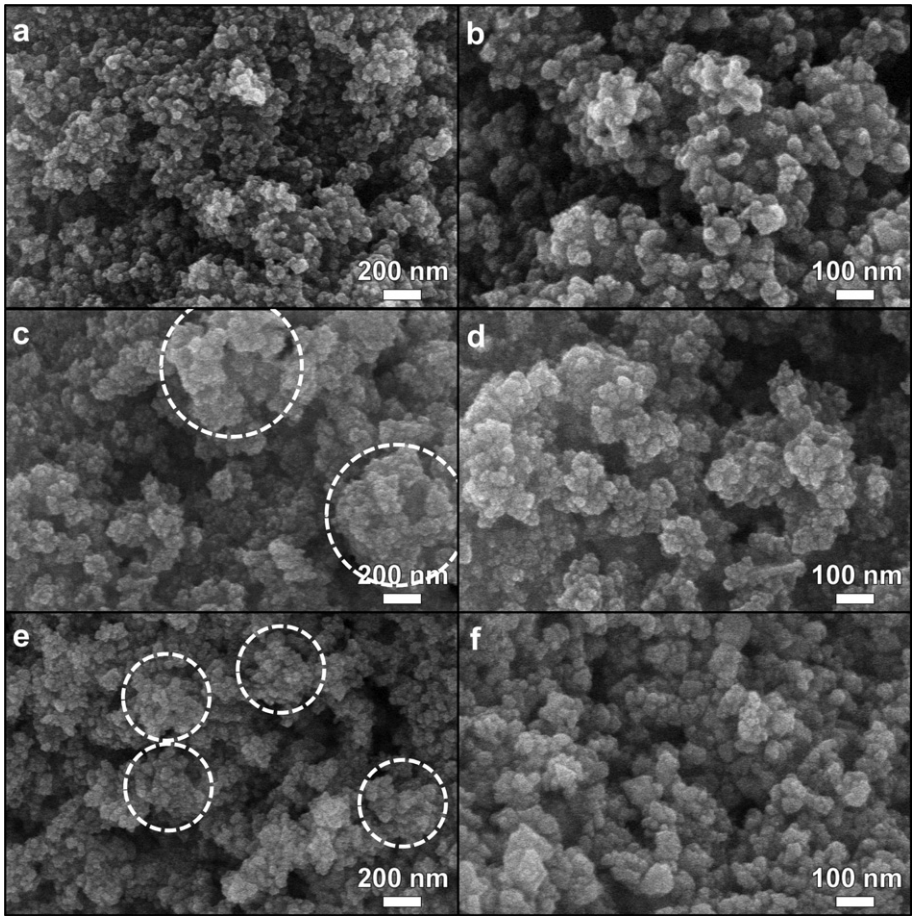

Fig. 2. SEM images of (a), (b) as-prepared carbonate precursors, (c), (d) GDC powders calcined at 700 °C for 2 h, and (e), (f) GDC powders calcined at 900 °C for 2 h.

After reduction of the NiO into metallic Ni, nickel felt connected with Ni wires (current collector) was fixed to the interior part of the tubular cell. Silver wire was wound around the cathode for current collection. H_2 humidified by bubbling water was flowed through the tubular cell at a rate of 250 cc min^{-1}, and air was flowed outside the tubular cell at a rate of 1.5 L min^{-1} while the cell performance was measured. The 2–3 cells were fabricated for each experimental condition and their power densities were similar.

2.4. Characterization of powders and cells

The phases and crystallinity of the powders were analyzed by X-ray diffraction (Rigaku, DMAX-II A, Cu Kα). A scanning electron microscope (SEM) (FE-SEM, Hitachi S-4800) was used to observe the powders and the cell structure. The *I–V* characteristics were measured by using a DC electric load. The complex impedance of the cell was measured using a high-frequency analyzer (Solartron-1260, Solartron Instruments, UK) with a Solartron-1287 interface (Solartron Instruments, UK) at frequencies from 10^{-2} to 10^{6} Hz. Signal amplitude was 100 mV.

3. Results and discussion

Fig. 1a shows the XRD pattern of the as-prepared carbonate precursor. After being heat-treated at 700 and 900 °C for 2 h, the powders were converted into crystalline GDC powders of the fluorite phase (Fig. 1b and c; JCPDS # 75-0161). The crystallite sizes of the GDC powders after heat treatment at 700 and 900 °C were determined to be 31.0 ± 1.2 nm and 52.8 ± 1.5 nm according to Scherrer's equation. This indicates that the crystallite coarsened at the higher calcination temperature.

The as-prepared carbonate precursors consist of small primary particles (size: 68 ± 9 nm) (Fig. 2a and b). The size of secondary particles (dotted circles in Fig. 2c and e) after heat treatment at 700 and 900 °C were approximately 600 and 400 nm, respectively. The size of the primary particles determined from the SEM image was decreased slightly to 34 ± 5 nm by heat treatment at 700 °C, which can be explained by decomposition of the carbonate precursors into oxide particles (Fig. 2d). Heat treatment at the higher calcination temperature (900 °C) increased the particle size to 60 ± 10 nm (Fig. 2f), which is consistent with the observation of crystallite coarsening in the X-ray diffraction results.

The apparent densities of the GDC pellets sintered at 1050–1400 °C for 5 h were measured by the Archimedes method, and the results are shown in Fig. 3. When the GDC powders calcined at 900 °C were used as raw materials, the apparent density increased with the sintering temperature up to 1200 °C and then tended to saturate at >1200 °C, although little fluctuation was observed. By contrast, the densification was significantly enhanced by decreasing the calcination temperature of the GDC powders to 700 °C. The density of the GDC pellet was as high as 6.9 even at the sintering temperature of 1050 °C and increased to 7.18 as the sintering temperature increased to 1200 °C. Considering the theoretical density of GDC (7.214 g cm^{-3}) [8], a GDC specimen with a relative density of >95% was prepared at 1050 °C in the present study.

The densification of ceramics closely depends on the starting powders and the compact configuration of the green body. To date,

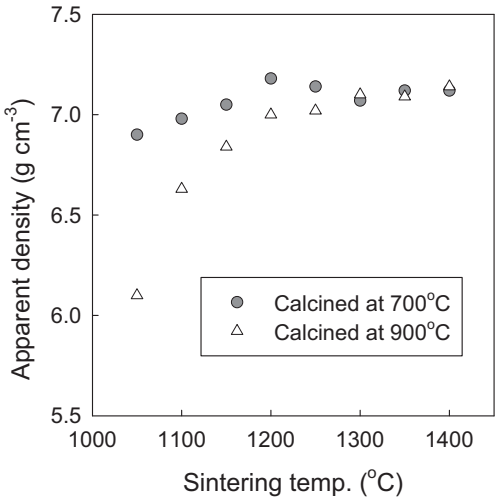

Fig. 3. Apparent densities of GDC specimens sintered at 1050–1400 °C for 5 h. The GDC powders calcined at 700 and 900 °C were used as raw materials.

various chemical routes for preparing highly pure and fine GDC powders have been suggested, including the solid-state reaction [9], combustion process [10,11], sol–gel process [12–14], hydrothermal process [15], and carbonate coprecipitation [7,16–18]. In particular, carbonate coprecipitation is known to be very effective for accomplishing full densification at low sintering temperatures. For example, Li et al. [19] reported the full densification of $Gd_{0.2}Ce_{0.8}O_{1.9}$ at a sintering temperature of 1100 °C. The densification of $Gd_{0.1}Ce_{0.9}O_{1.95}$ at a relatively low sintering temperature in the present study can also be attributed to the highly active starting powders prepared by carbonate coprecipitation.

After dip coating of the GDC layer on the NiO-YSZ support/NiO/NiO-GDC, the tubular structures were sintered at 1300–1400 °C for 5 h. The GDC layers were significantly cracked and delaminated when GDC powders calcined at 700 °C were used. In contrast, impermeable GDC layers could be fabricated using the GDC powders calcined at 900 °C. The laminated structure may be cracked or delaminated when either the final amounts of shrinkage at the sintering temperature or the shrinkage rates during the densification of the two heterolayers are significantly different from each other. Regardless of calcination temperature, the GDC densities of specimens sintered at 1300–1400 °C are similar (Fig. 3), indicating that the cracking and delamination found in the specimen using the powders calcined at 700 °C result from the shrinkage mismatch during densification. Accordingly, the powders calcined at 900 °C were used to fabricate the tubular SOFC cell.

The configurations of the tubular cells are shown in Fig. 4. A NiO–YSZ tube (length, ~8 cm; outer diameter, 7.5 mm; inner diameter, 4.9 mm) was used as a support (Fig. 4a), and it was coated with NiO–GDC layers to form the anode. Highly resistive second phases such as $Ce_{0.37}Zr_{0.38}Gd_{0.18}Y_{0.70}O_{1.87}$ are known to form at the interface between YSZ and $Gd_{0.2}Ce_{0.8}O_{1.9}$ through the interdiffusion of Y, Zr, Gd, and Ce above 1200 °C [20,21]. Thus, the NiO functional layer was formed between the NiO–YSZ support and the NiO–GDC anode layer in order to prevent the formation of a resistive second phase and to enhance the bonding between the NiO–YSZ and NiO–GDC layers. After the NiO functional layer and NiO–GDC anode layer were coated, the GDC layers were dip-coated and subsequently heated to 400 °C (Fig. 4b). The shrinkage of the NiO–YSZ/NiO/NiO–GDC/GDC tubes after sintering at 1400 °C was ~25% (Fig. 4c). Bilayers of LSCF–GDC and LSCF were coated on the GDC to increase the length of the triple phase boundary, and the cell was reduced in H_2 at 600 °C to convert all the NiO components of the cell into metallic Ni (Fig. 4d). The entire cell configuration for measurement is shown in Fig. 4e. The active cell areas of tubular cells prepared by sintering at 1350 and 1400 °C were calculated by the outer diameter and length of cathode area, which were 3.95 and 3.77 cm^2, respectively. The thicknesses of the final cells were similar (1.20 mm).

Many pores were frequently observed on the top surface of the GDC electrolytes sintered at 1350 °C (Fig. 5a), while most surface pores were eliminated when the sintering temperature was increased to 1400 °C (Fig. 5b). Cross-sectional images of the cells are shown in Fig. 6. In the high-magnification images of the GDC layers, the numbers and total cross-sectional area of pores were decreased as increasing the sintering temperature from 1350 °C to 1400 °C, indicating that the density of the GDC specimen sintered at 1350 °C is lower than that sintered at 1400 °C (Fig. 6b and d). As shown in Fig. 3, the shrinkage in the temperature regime between 1350 and 1400 °C can be regarded as very small. This indicates that a shrinkage mismatch between different layers is a more plausible reason explaining the development of the porous microstructure at the sintering temperature of 1350 °C. After reduction in H_2 at 600 °C, all the interfaces were distinct, except that between LSCF and LSCF–GDC. The thicknesses of the Ni functional layer, Ni–GDC anode layer, GDC layer, and LSCF–GDC/LSCF cathode bilayer of the cell were 13, 11, 21, and 23 μm after sintering at 1350 °C and 15, 13, 22, and 21 μm after sintering at 1400 °C, respectively (Fig. 6a and c).

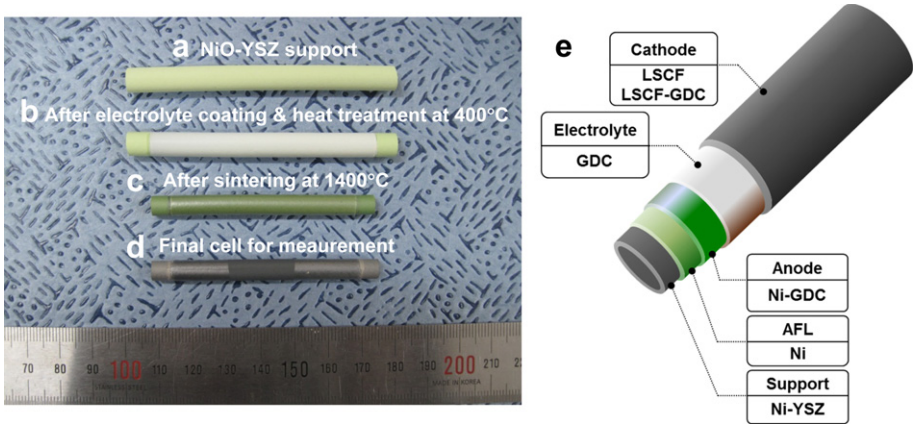

Fig. 4. Images of (a) NiO–YSZ support, (b) NiO–YSZ/NiO/NiO–GDC/GDC tube before sintering, (c) NiO–YSZ/NiO/NiO–GDC/GDC tube after sintering at 1400 °C for 5 h, and (d) Ni–YSZ/Ni/Ni–GDC/GDC/LSCF–GDC/LSCF cell for measurement after reduction in hydrogen atmosphere at 600 °C for 3 h. (e) Schematic structure of tubular SOFC cell.

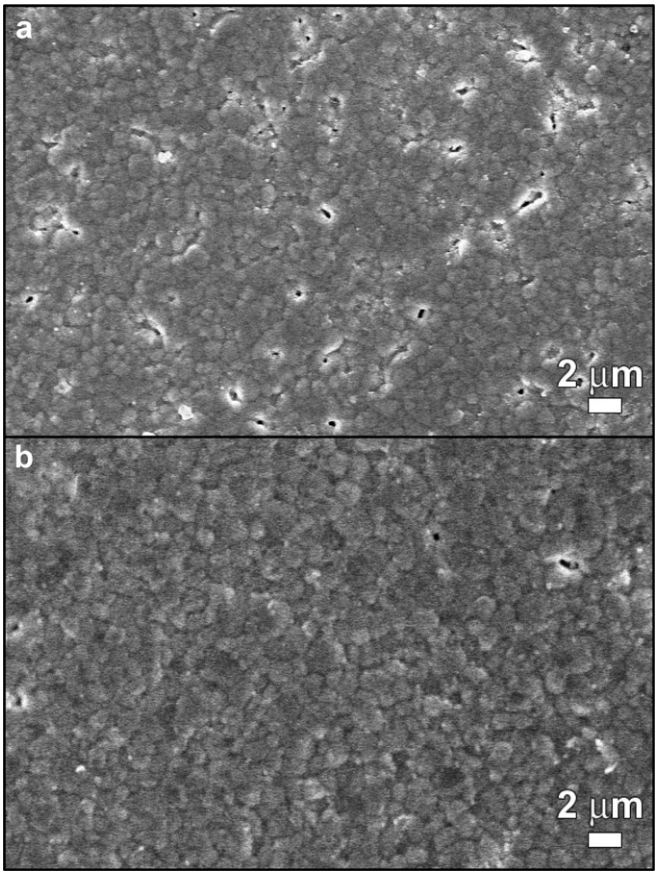

Fig. 5. Top-view SEM images of GDC electrolyte layers sintered at (a) 1350 °C and (b) 1400 °C.

The matching of thermal expansion coefficients (TEC) for the layers is important to decrease the thermal shock of SOFC cell during the operation. The TEC values of YSZ, Ni, GDC, and LSCF reported in the literature are 11.0×10^{-6} K^{-1} [22,23], 17.0×10^{-6} K^{-1} [22,23], 12.6×10^{-6} K^{-1} [24], and 15.3×10^{-6} K^{-1} [25], respectively. From the rule of mixture, the TEC values of the Ni–YSZ, Ni–GDC, and LSCF–GDC layers in the present study were calculated to be 14.6×10^{-6} K^{-1}, 14.3×10^{-6} K^{-1}, and 14.0×10^{-6} K^{-1}, respectively. Considering that Ni functional is relatively thin, most layers in the present cell show comparable TEC values.

Fig. 7 shows the *I–V* and *I–P* characteristics of the cells at operation temperatures of 450–600 °C. The cell sintered at 1350 °C showed an open-circuit voltage (OCV) of 1.0 V at the operation temperature of 450 °C, and the OCV values decreased slightly to 0.87 V as the operation temperature increased to 600 °C (Fig. 7a). The OCV values of the cell are lower than the theoretical value at 600 °C (~1.1 V). The maximum power densities of the cell were 72, 134, 233, and 350 mW cm^{-2} at the operation temperatures of 450, 500, 550, and 600 °C, respectively. The OCV values of the cell sintered at 1400 °C decreased from 0.94 to 0.84 V as the operation temperature increased from 450 to 600 °C. The maximum power densities of the cell at 450, 500, 550, and 600 °C were 141, 288, 445, and 594 mW cm^{-2}, respectively, which were substantially higher than those of the cell sintered at 1350 °C. In general, lower OCV values are frequently found for GDC electrolyte, which can be explained by the potential drop due to the contribution of electronic conduction in a highly reducing atmosphere [26,27].

The impedance spectra of the cells under the open-circuit condition were measured at 450–600 °C (Fig. 8). The ohmic resistance (R_b), electrode resistance (R_e), and total resistance (R_t) of the cell were determined from the impedance spectra, and the results are plotted in Fig. 9. The R_b values of the cell prepared by sintering at 1350 °C gradually decreased from 1.72 to 0.87 Ω cm^2 as the

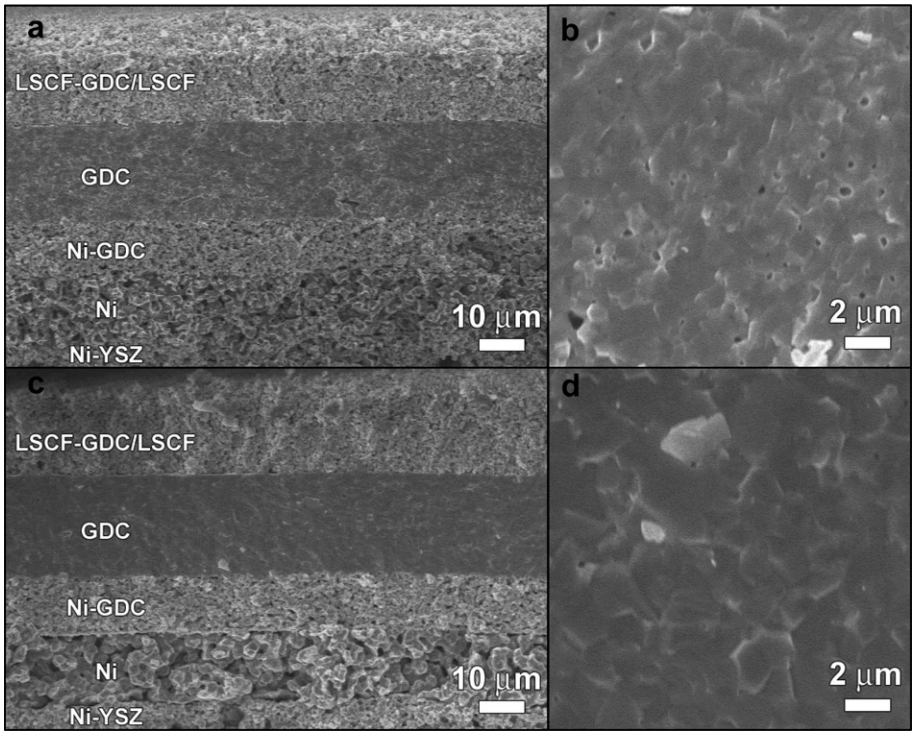

Fig. 6. Cross-sectional SEM images of the cell structures and GDC electrolyte layers: (a), (b) cell prepared by sintering the electrolyte at 1350 °C and (c), (d) cell prepared by sintering the electrolyte at 1400 °C.

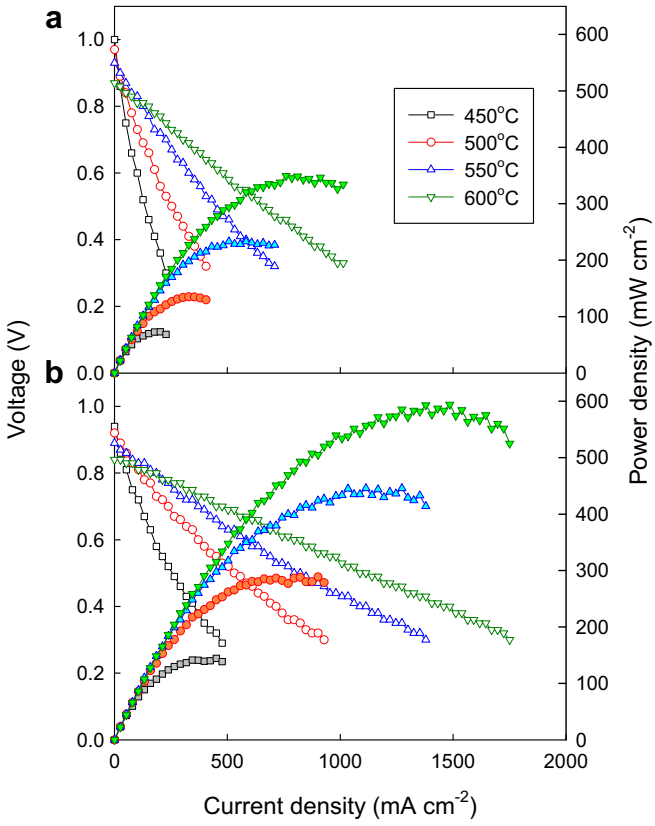

Fig. 7. *I*–*V* and *I*–*P* graphs for the cells prepared by sintering the electrolyte layer at (a) 1350 °C and (b) 1400 °C.

operation temperature increased from 450 to 600 °C (Fig. 9a). In contrast, the R_e values drastically decreased from 5.34 to 0.09 Ω cm^2 (Fig. 9a), probably because of the thermal promotion of the electrode reaction. When the sintering temperature was elevated to 1400 °C, both the R_b and R_e values at 450–600 °C became lower, whereas the tendencies for the R_b and R_e values to vary as a function of operation temperature remained similar (Fig. 9b). Accordingly, in both cells, the total resistance of the cell is dominated by the contribution of R_e at 450 °C and by the contribution of R_b at 600 °C.

Note that the R_e values of the cell sintered at 1350 °C are 1.6–2.2 times higher than those of the cell sintered at 1400 °C. In general, the electrode polarization of conventional SOFCs is dominated by cathode polarization [28]. The thicknesses and configurations of the cathode layers can be regarded as similar, because the dip-coating procedures were carefully conducted after reproducible processing conditions were confirmed although the thickness of the LSCF–GDC composite layer could not be measured precisely because of the indistinct demarcation between the LSCF–GDC and LSCF layers. This indicates that the R_e values are determined by the configurations of the interfaces between LSCF–GDC and GDC. Taking into account the higher number of surface defects on the surfaces of the GDC electrolyte layers sintered at 1350 °C (Fig. 5a), the higher R_e values in Fig. 9a can be explained by the relatively poor adherence between the electrolyte and electrode layers and the consequent decrease in the triple phase boundary length. As shown in Fig. 9, the contribution of electrode polarization at 600 °C to the total resistance is very small, indicating that the use of a highly conductive electrolyte is more advantageous for enhancing the power density of the cell. When the cell is operated at ≤500 °C, by contrast, the power density can be improved by designing high-performance electrodes with lower electrode polarizations.

The anode materials, electrolytes, cathode materials, cell diameters, operation temperatures, and power densities of the tubular SOFCs reported in the literature are summarized in Table 1 [4,29–50]. Most of the Ni–YSZ anode-supported tubular SOFCs using YSZ electrolytes required high operation temperatures (>800 °C), probably because of the low ionic conductivity of YSZ, and their maximum power densities ranged from 377 to

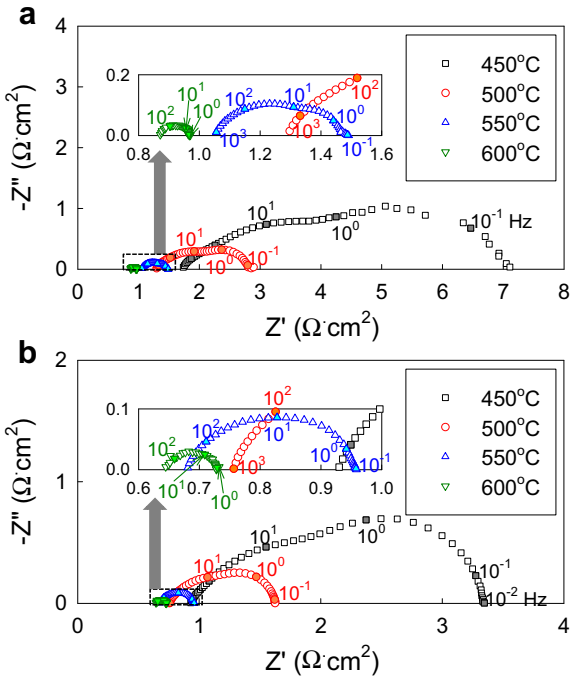

Fig. 8. Impedance spectra of the cells at 450–600 °C: (a) cell prepared by sintering the electrolyte at 1350 °C and (b) cell prepared by sintering the electrolyte at 1400 °C.

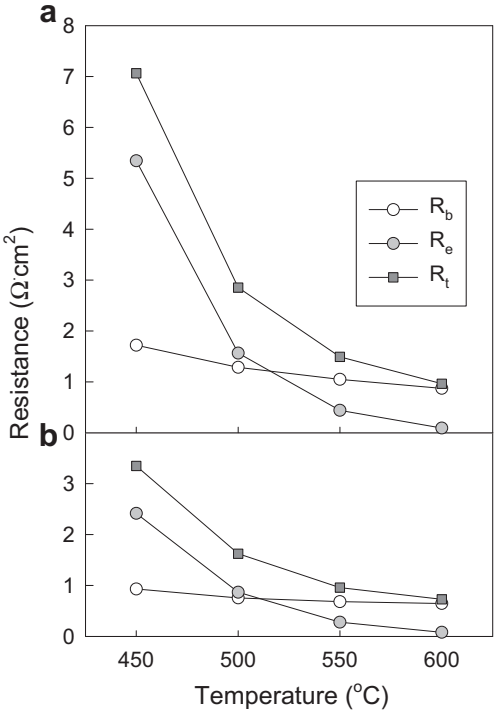

Fig. 9. Area-specific resistances of the electrolyte (R_b), electrode (R_e), and entire cells (R_t) at 450–600 °C: (a) cell prepared by sintering the electrolyte at 1350 °C and (b) cell prepared by sintering the electrolyte at 1400 °C.

Table 1
Single-cell performance of tubular SOFCs using hydrogen as fuel.

Support/anode	Electrolyte	Cathode	Cell diameter (mm)	Temp. (°C)	Power density (mW cm^{-2})	Ref.
Ni–YSZ	YSZ	LSM[a]/LSCF[b]	10	800	540	[29]
Ni–YSZ	YSZ	PNSM[c]–YSZ	7	850	415	[30]
Ni–YSZ	YSZ	LSM[a]–SDC[d]	6.2	800	483	[31]
Ni–YSZ	YSZ	LSM[e]–YSZ	5.72	850	907	[32]
Ni–YSZ	YSZ	LSCM[f]–SDC[d]–YSZ	2.5	850	513	[33]
Ni–YSZ	YSZ	PNSM[c]–YSZ	2.5	800	459	[34]
Ni–YSZ	YSZ	LSM[g]–SDC[d]	2	800	752	[35]
Ni–YSZ	YSZ	LSM[h]–YSZ/LSM[h]	2	750	400	[36]
Ni–YSZ	YSZ	LSM–YSZ	1.7	800	377	[37]
Ni–YSZ	YSZ	LSCF[b]–GDC	1.7	600	390	[38]
Ni–YSZ/Ni–ScSZ[i]	ScSZ[i]	LSM[j]–ScSZ[i]	10	850	405	[39]
Ni–YSZ/Ni–ScSZ	ScSZ	LSM	10	850	433	[40]
Ni–YSZ/Ni–ScSZ[k]	ScSZ[k]	LSCF[b]–GDC	1.93	700	570	[41]
Ni–YSZ	ScSZ	LSCF[b]–GDC	1.8	700	690	[42]
Ni–YSZ/Ni–GDC	GDC	LSCF[b]–GDC/LSCF[b]	6	600	597	This study
				550	445	
				500	288	
				450	141	
Ni–GDC[l]	GDC[l]	LSCF[b]–GDC[l]	1.8	550	1310	[43]
Ni–GDC[l]	GDC[l]	LSCF[b]–GDC[l]	1.8	550	340	[44]
Ni–GDC[l]	GDC[l]	LSCF[b]–GDC[l]	1.8	500	350	[45]
Ni–GDC	GDC	LSCF[b]–GDC	1.5	550	400	[46]
Ni–GDC[l]	GDC[l]	LSCF[b]–GDC[l]	0.8	550	1017	[4]
Ni–GDC	GDC	LSCF[m]–GDC	0.8	550	350	[47]
Ni–GDC	GDC	LSCF[b]–GDC	3	450	66	[48]
Ni–BZCYYb[n]	BZCYYb	LSCF[b]–BZCYYb	3	600	260	[49]
Ni–BZCYYb	BZCYYb	SSC[o]–BZCYYb	2.5	650	254	[50]

[a] LSM: $(La_{0.85}Sr_{0.15})_{0.9}MnO_{3-\delta}$.
[b] LSCF: $La_{0.6}Sr_{0.4}Co_{0.2}Fe_{0.8}O_{3-\delta}$.
[c] PNSM: $(Pr_{0.26}Nd_{0.74})_{0.7}Sr_{0.3}MnO_3$.
[d] SDC: $Sm_{0.2}Ce_{0.8}O_{1.9}$.
[e] LSM: $La_{0.7}Sr_{0.3}MnO_3$.
[f] LSCM: $(La_{0.75}Sr_{0.25})_{0.95}Cr_{0.5}Mn_{0.5}O_{3-\delta}$.
[g] LSM: $La_{0.85}Sr_{0.15}MnO_3$.
[h] LSM:$(La_{0.8}Sr_{0.2})_{0.95}MnO_3$.
[i] ScSZ: $Zr_{0.89}Sc_{0.1}Ce_{0.01}O_{2-\delta}$.
[j] LSM: $(La_{0.8}Sr_{0.2})_{0.98}MnO_3$.
[k] ScSZ: 10 mol% Sc_2O_3-stabilized ZrO_2.
[l] GDC: $Gd_{0.2}Ce_{0.8}O_{1.9}$.
[m] LSCF: $La_{0.8}Sr_{0.2}Co_{0.6}Fe_{0.4}O_3$.
[n] BZCYYb: $BaZr_{0.1}Ce_{0.7}Y_{0.1}Yb_{0.1}O_{3-\delta}$.
[o] SSC: $Sm_{0.5}Sr_{0.5}CoO_3$.

907 mW cm^{-2} [29–35,37]. When scandia-stabilized zirconia (ScSZ, Sc_2O_3-stabilzied ZrO_2), which has a higher ionic conductivity, was used as the electrolyte, the cell operation temperatures tended to decrease. The maximum power density of 690 mW cm^{-2} has been reported at operation temperature of 700 °C [42].

The maximum power density of the present cell is 594 mW cm^{-2} at 600 °C. This is one of the highest values among the Ni–YSZ-supported SOFCs in the literature, if one takes into account the fact that the power density tended to decrease as the operation temperature of the SOFC decreased. The power density of 445 mW cm^{-2} at 550 °C in the present study is also comparable to those of micro-tubular SOFCs supported by Ni–GDC anodes with diameters of 0.8–1.8 mm (350–1310 mW cm^{-2}) [4,43–47]. Considering that the power density of tubular SOFCs is inversely proportional to the tube diameter, the power density of the present cell with a diameter of 6 mm can be regarded as sufficiently high. The SOFC using a Ni–YSZ support tube with a manipulable diameter in the present study provides various advantages for commercialization of low-temperature and intermediate-temperature SOFCs, such as excellent mechanical strength of the support, stable operation of the cell, and cost-effective Ni–YSZ component materials, without significant deterioration of the power density.

In general, the GDC electrolyte layers of SOFCs are sintered at ≥1400 °C. In order to explore the possibility of lowering the sintering temperature, a tubular cell was fabricated by sintering the GDC layer at 1300 °C, and the cell performance was measured at 450–600 °C (Figs. 10 and 11). The configuration and thickness of the final cell were similar to those of the cells prepared by sintering the electrolyte at 1350 and 1400 °C. The active cell areas of the tubular cells prepared by sintering the electrolyte at 1300 °C were 3.93 cm^2. The thicknesses of the Ni functional layer, Ni–GDC anode layer, GDC layer, and LSCF–GDC/LSCF cathode bilayer of the cell were 13, 11, 21, and 13 μm, respectively (Fig. 10b). The thicknesses of most layers were similar to those in the previous cases, although the cathode layer was slightly thinner. The large number of surface cracks (Fig. 10a) and the porosity within the electrolyte (Fig. 10b,c) can be attributed to the shrinkage mismatch between the electrolyte layer and the NiO–YSZ support. The cell sintered at 1300 °C showed an OCV of 0.83 V and a maximum power density of 179 mW cm^{-2} at the operation temperature of 600 °C (Fig. 11). This clearly demonstrates that the sintering temperature of tubular SOFCs can be decreased down to 1300 °C.

In the present study, a GDC specimen with a 97% relative density was obtained using the carbonate-derived GDC powders even at 1200 °C. However, the shrinkage mismatch between the Ni–YSZ and GDC due to the additional shrinkage of the Ni–YSZ support above 1200 °C led to the formation of surface cracks and pores in the GDC electrolytes sintered at 1300 and 1350 °C. The shrinkage of the Ni–YSZ support can be tuned by proper control of the Ni

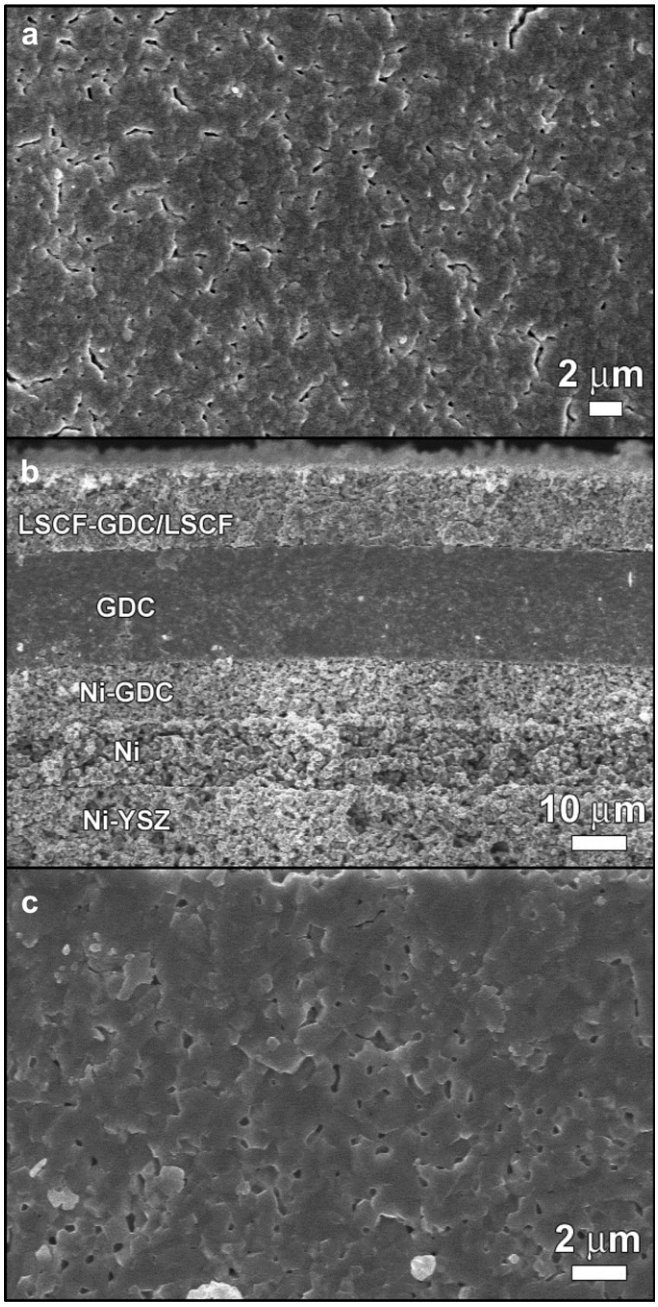

Fig. 10. Top-view and cross-sectional SEM images of the cell prepared by sintering the electrolyte at 1300 °C: (a) Top-view SEM image of GDC electrolyte layer, (b) cross-sectional SEM image of the cell, and (c) cross-sectional SEM image of GDC electrolyte layers.

particle sizes [51], YSZ particle sizes [52], sintering additives [53], pore former [54] and pre-sintering temperature [36] of the Ni–YSZ green body. A GDC specimen with a 95% relative density could be obtained at a sintering temperature as low as 1050 °C by using the GDC powders calcined at 700 °C. Accordingly, the co-firing temperature of the tubular cell in the present study may be decreased down to 1050 °C if the shrinkage of the Ni–YSZ support can be controlled. This indicates that the cell structure can be simplified by removing the NiO functional layers between the NiO–YSZ support and the NiO–GDC anode and that the formation of resistive interfacial phases by interlayer cation diffusion between YSZ and GDC at >1200 °C [21,22] can be prevented.

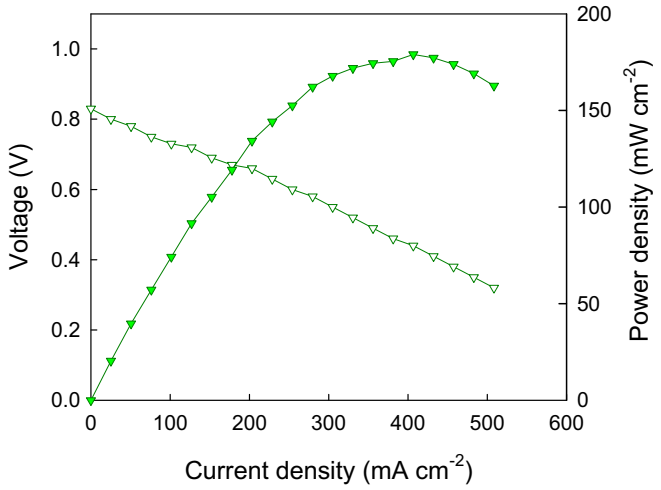

Fig. 11. *I–V* and *I–P* graphs measured at 600 °C of the cells prepared by sintering the electrolyte layer at 1300 °C.

4. Conclusions

Ni–YSZ-supported tubular SOFCs with a cell configuration of Ni–YSZ/Ni/Ni–GDC/GDC/LSCF–GDC/LSCF were fabricated using highly sinterable GDC powders prepared by carbonate coprecipitation. The cell prepared by sintering of GDC electrolyte at 1400 °C showed a high maximum power density (594 mW cm^{-2}) at an operation temperature of 600 °C, while the power densities decreased to 179 and 350 mW cm^{-2} when the electrolytes were sintered at 1300 and 1350 °C, respectively. The higher power density of the cell sintered at 1400 °C was attributed the dense electrolyte and good adherence between the electrolyte and electrodes due to the shrinkage matching of the NiO–YSZ/NiO/NiO–GDC/GDC tubular structure during co-firing. The co-firing temperature can be lowered by tuning the shrinkage of the NiO–YSZ support, which may allow further simplification of the cell structures and reduce the reactivity between electrolyte and electrode. The present tubular SOFCs using Ni–YSZ supports with manipulable diameters provide various advantages for commercialization, such as excellent mechanical strength of the support, stable operation of the cell, and cost-effective component materials without significant deterioration of the power density.

Acknowledgments

This work was supported by the New and Renewable Energy R&D Program (20093020030040) under the Korea Ministry of Knowledge Economy (MKE).

References

[1] S.C. Singhal, Solid State Ionics 135 (2000) 305–313.
[2] N.M. Sammes, Y. Du, R. Bove, J. Power Sources 145 (2005) 428–434.
[3] B.C.H. Steele, J. Mater. Sci. 36 (2001) 1053–1068.
[4] T. Suzuki, Y. Funahashi, T. Yamaguchi, Y. Fujishiro, M. Awano, Solid State Ionics 180 (2008) 546–549.
[5] M. Sahibzada, B.C.H. Steele, K. Zheng, R.A. Rudkin, I.S. Metcalfe, Catal. Today 38 (1997) 459–466.
[6] M. Sahibzada, B.C.H. Steele, D. Barth, R.A. Rudkin, I.S. Metcalfe, Fuel 78 (1999) 639–643.
[7] J.-G. Li, T. Ikegami, T. Mori, T. Wada, Chem. Mater. 13 (2001) 2913–2920.
[8] E. Suda, B. Pacaud, Y. Montardi, M. Mori, M. Ozawa, Y. Takeda, Electrochemistry 71 (2003) 866–872.
[9] Z. Khakpour, A.A. Youzbashi, A. Maghsoudipour, K. Ahmadi, Powder Technol. 214 (2011) 117–121.
[10] L.D. Jadhav, M.G. Chourashiya, K.M. Subhedar, A.K. Tyagi, J.Y. Patil, J. Alloys Compd. 470 (2009) 383–386.

[11] T. Mahata, G. Das, R.K. Mishra, B.P. Sharma, J. Alloys Compd. 391 (2005) 129–135.
[12] Y. Tao, J. Shao, J. Wang, W.G. Wang, J. Alloys Compd. 484 (2009) 729–733.
[13] D.H. Prasad, J.-W. Son, B.-K. Kim, H.-W. Lee, J.-H. Lee, J. Eur. Ceram. Soc. 28 (2008) 3107–3112.
[14] K. Huang, M. Feng, J.B. Goodenough, J. Am. Ceram. Soc. 81 (1998) 357–362.
[15] S. Dikmen, P. Shuk, M. Greenblatt, H. Gocmez, Solid State Sci. 4 (2002) 585–590.
[16] J.-G. Li, T. Ikegami, Y. Wang, T. Mori, J. Am. Ceram. Soc. 86 (2003) 915–921.
[17] J.-G. Li, T. Ikegami, Y. Wang, T. Mori, J. Am. Ceram. Soc. 85 (2002) 2376–2378.
[18] A.I.Y. Tok, L.H. Luo, F.Y.C. Boey, Mater. Sci. Eng. A 383 (2004) 229–234.
[19] J.-G. Li, T. Ikegami, T. Mori, T. Wada, Chem. Mater. 13 (2001) 2921–2927.
[20] A. Tsoga, A. Gupta, A. Naoumidis, D. Skarmoutsos, P. Nikolopoulo, Ionics 4 (1998) 234–240.
[21] A. Tsoga, A. Naoumidis, D. Stöver, Solid State Ionics 135 (2000) 403–409.
[22] S. Primdahl, M. Mogensen, J. Electrochem. Soc. 144 (1997) 3409–3419.
[23] S.K. Pratihar, A.D. Sharma, R.N. Basu, H.S. Maiti, J. Power Sources 129 (2004) 138–142.
[24] H. Hayashi, M. Kanoh, C.J. Quan, H. Inaba, S. Wang, M. Dokiya, H. Tagawa, Solid State Ionics 132 (2000) 227–233.
[25] G. Corbel, S. Mestiri, P. Lacorre, Solid State Sci. 7 (2005) 1216–1224.
[26] B.C.H. Steele, Solid State Ionics 129 (2000) 95–110.
[27] K. Eguchi, T. Setoguchi, T. Inoue, H. Arai, Solid State Ionics 52 (1992) 165–172.
[28] A. Bieberle-Hütter, D. Beckel, A. Infortuna, U.P. Muecke, J.L.M. Rupp, L.J. Gauckler, S. Rey-Mermet, P. Muralt, N.R. Bieri, N. Hotz, M.J. Stutz, D. Poulikakos, P. Heeb, P. Müller, A. Bernard, R. Gmür, T. Hocker, J. Power Sources 177 (2008) 123–130.
[29] S.-B. Lee, T.-H. Lim, R.-H. Song, D.-R. Shin, S.-K. Dong, Int. J. Hydrogen Energy 33 (2008) 2330–2336.
[30] M. Liu, J. Gao, D. Dong, X. Liu, G. Meng, Int. J. Hydrogen Energy 35 (2010) 10489–10494.
[31] L. Zhang, J. Gao, M. Liu, C. Xia, J. Alloys Compd. 482 (2009) 168–172.
[32] J. Ding, J. Liu, W. Yuan, Y. Zhang, J. Eur. Ceram. Soc. 28 (2008) 3113–3117.
[33] X. Zhang, B. Lin, Y. Ling, Y. Dong, G. Meng, X. Liu, Int. J. Hydrogen Energy 35 (2010) 8654–8662.
[34] X. Zhang, B. Lin, Y. Ling, Y. Dong, G. Meng, X. Liu, J. Alloys Compd. 497 (2010) 386–389.
[35] C. Chen, M. Liu, L. Yang, M. Liu, Int. J. Hydrogen Energy 36 (2011) 5604–5610.
[36] N. Shikazono, Y. Sakamoto, Y. Yamaguchi, N. Kasagi, J. Power Sources 193 (2009) 530–540.
[37] C. Yang, W. Li, S. Zhang, L. Bi, R. Peng, C. Chen, W. Liu, J. Power Sources 187 (2009) 90–92.
[38] T. Suzuki, M.H. Zahir, T. Yamaguchi, Y. Fujishiro, M. Awano, N. Sammes, J. Power Sources 195 (2010) 7825–7828.
[39] R. Liu, C. Zhao, J. Li, S. Wang, Z. Wen, T. Wen, J. Power Sources 195 (2010) 541–545.
[40] R. Liu, G. Cai, J. Li, C. Zhao, S. Wang, T. Wen, Z. Wen, J. Solid State Electrochem. 14 (2010) 1923–1928.
[41] T. Suzuki, B. Liang, T. Yamaguchi, H. Sumi, K. Hamamoto, Y. Fujishiro, J. Power Sources 199 (2012) 170–173.
[42] T. Suzuki, Y. Takahashi, K. Hamamoto, T. Yamaguchi, Y. Fujishiro, Int. J. Hydrogen Energy 36 (2011) 10998–11003.
[43] F. Calise, G. Restucccia, N. Sammes, J. Power Sources 195 (2010) 1163–1170.
[44] T. Yamaguchi, K.V. Galloway, J. Yoon, N.M. Sammes, J. Power Sources 196 (2011) 2627–2630.
[45] M.H. Zahir, T. Suzuki, Y. Funahashi, T. Yamaguchi, Y. Fujishiro, M. Awano, Fuel Cells 9 (2009) 164–169.
[46] T. Yamaguchi, T. Suzuki, S. Shimizu, Y. Fujishiro, M. Awano, J. Membr. Sci. 300 (2007) 45–50.
[47] T. Suzuki, T. Yamaguchi, Y. Fujishiro, M. Awano, J. Power Sources 160 (2006) 73–77.
[48] V. Gil, J. Gurauskis, R. Campana, R.I. Merino, A. Larrea, V.M. Orera, J. Power Sources 196 (2011) 1184–1190.
[49] L. Zhao, X. Zhang, B. He, B. Liu, C. Xia, J. Power Sources 196 (2011) 962–967.
[50] F. Zhao, C. Jin, C. Yang, S. Wang, F. Chen, J. Power Sources 196 (2011) 688–691.
[51] R. Ueyama, T. Ueyama, K. Koumoto, K. Kuribayashi, J. Ceram. Soc. Jpn. 109 (2001) 661–666.
[52] L. Jia, Z. Lu, J. Miao, Z. Liu, G. Li, W. Su, J. Alloys Compd. 414 (2006) 152–157.
[53] T.A.G. Restivo, S.D.H. Mello-Castanho, J. Power Sources 185 (2008) 1262–1266.
[54] A. Sanson, P. Pinasco, E. Roncari, J. Eur. Ceram. Soc. 28 (2008) 1221–1226.